Title
HIGH VOLTAGE, HIGH RESOLUTION ELECTRON MICROSCOPY IN MATERIALS RESEARCH

Author
Thorns, G.

Publication Date
1986-12-01

Lawrence Berkeley Laboratory
UNIVERSITY OF CALIFORNIA

Materials & Molecular Research Division

Submitted to Journal de Microscopie et de Spectroscopie Electroniques

HIGH VOLTAGE, HIGH RESOLUTION ELECTRON MICROSCOPY IN MATERIALS RESEARCH

G. Thomas

December 1986

Prepared for the U.S. Department of Energy under Contract DE-AC03-76SF00098

DISCLAIMER

HIGH VOLTAGE, HIGH RESOLUTION ELECTRON MICROSCOPY IN MATERIALS RESEARCH+

Gareth THOMAS
Scientific Director,
National Center for Electron Microscopy
Lawrence Berkeley Laboratory and
Professor, Materials Science
University of California
Berkeley, CA 94720

ABSTRACT

This paper is a brief summary of the current status of high resolution atomic imaging capabilities at the National Center for Electron Microscopy, Berkeley. Examples of research problems in semiconductors and alloys and the image computation and simulation systems are described.

INTRODUCTION

It is an honour and a pleasure to contribute this brief article in memory of the late Professor Gaston Dupouy. M. Dupouy had a profound influence on electron microscopy and science in general and on my own research in particular. He pioneered high voltage electron microscopy (e.g., Ref. 1) and was a perfectionist. One wonders where the field would be today if he had not built the first (1.2MeV) machine in the early 1960s.

The early work in high voltage microscopy led me to considering the possibilities of using HVEM in materials science, especially to go beyond metallurgy into ceramics and minerals. I was delighted to be accepted at Toulouse to do some rather simple experiments on penetration and ionisation damage, first in 1967 and again in 1972 when the 3MeV microscope became

+Dedicated to the memory of Professor Gaston Dupouy.

available [2,3]. These visits were significant in our efforts to establish the National Center for Electron Microscopy (which finally materialized in 1983) after the installation of our first HVEM, a 650kV microscope in 1969. An important, amusing factor which contributed to my acceptance by Gaston Dupouy to work in Toulouse was probably our mutual love of rugby football as I was careful to wear my "Stade Toulousaine" button on my first interview with him. This button was a souvenir of a tough encounter on the rugby field for a touring Cambridge University XV, years before. From our first meeting in 1962, M. Dupuoy was a marvelous host and friend to me and my family.

Professor Dupouy's impact on HVEM in particular and on its applications in general can be measured partly by the specialized conferences on these topics and the evergrowing utilization of HVEM instruments in scientific research, typified by recent conference reports (4-6).

2. Basis for HVEM and the NCEM at Berkeley

The main reasons for using higher voltage microscopes for research applications (see Table 1) are well known, e.g., improved resolution, penetration, the ability to carry out in-situ experiments in controlled environments, reduced ionisation damage (but increasing probability of knock-on displacement damage and hence the need for a variable voltage instrument), special diffraction effects such as critical voltage, improved resolution in amplitude contrast, inversion voltage (7) and improved resolution for microanalysis typified by the work of Jouffrey et al. on EELS (8).

After the departure from the field of transmission electron and microanalytical microscopy by U.S. manufacturers in the early 1970s, it became clear that a national effort was required to maintain state-of-the-art standards for this instrumentation. With the development of specialized and expensive equipment, mostly from Europe and Japan, and the need for specialized knowledge for operation and maintenance, the user-oriented

Table 1
Outline of Developments of TEM in Materials Science Research

Year	Specimens	Applications/Developments	Instrumentation	Resolution+
1940/50	Replicas 1. Oxide 2. Carbon 3. Plastics	Surfaces Slip steps Extracted particles Fractography	50kV instruments Single condenser Little or no theory	~100Å
1949--Heidenreich published first paper on TEM of thin foils; basic theory outlined				
1950/60	Thin foil techniques 1. From bulk 2. Deposited	Defects Phase transitions	100kV instruments, contrast theory developed	~ 5Å-20Å
Many developments in instrumentation, specimen preparation methods, and image contrast and diffraction theory for interpretation of data				
1969/70	Metals Non-metals, semiconductors Ceramics (ion thinning) Minerals	Dynamic, in-situ studies: Information explosion on substructure of solids Microdiffraction	First HVEM built in Toulouse (1.2MeV); first 3MeV HVEM built in Toulouse; accessories for in-situ studies; controlled experiments	3Å
1970/80	As above Catalysts	Theories for high resolution interpretation developed	TEM/STEM analytical, convergent beam; spectroscopy EDXS, EELS commercial HVEMs 0.5-1.5MeV; general acceptance	2Å
Structure imaging to ~2Å interpretable resolution; lattice imaging widely used				
1980/90	Virtually all materials	Atomic resolution in close-packed solids; surface imaging, small particles; fast computation facilities for interpretation, simulation	Medium voltage HREM/AEM(100-400eV commercially available; improved analytical capabilities; parallel detection in EELS wide-spread applications in all fields; UHV microscopes	1.5Å

+Interpretable point-to-point

National Center for Electron Microscopy was established following the earliest proposals to the Government and the scientific support resulting from a National Workshop held in 1976. The Materials Science Division (Office of Basic Energy Sciences) of the Department of Energy provided funding and support for the National Center at the Lawrence Berkeley Laboratory, University of California. The facility was built over a three-year period and was formally dedicated in September 1983. As a user facility, it is open to qualified scientists with research projects of interest to DOE. Proposals to use the electron microscopes are reviewed and approved by the Steering Committee which draws members from industry, national laboratories and universities. All proposals are judged solely on their scientific merit.

At the heart of the facility are two high voltage electron microscopes: the JEOL JEM ARM-1000 and KRATOS EM 1500, the highest voltage microscope in the U.S.A. In addition there are conventional 200kV instruments for high resolution and microanalytical applications. The Center also provides computing, image simulation and processing capabilities (see Sec. 5).

3. Atomic Resolution Microscopy

It has long been the goal of electron microscopists to achieve interpretable resolution at the atomic level. The resolution is fundamentally a function of electron wavelength and lens aberrations, especially spherical aberration C_s, according to the relationship:

$$R = 0.66 C_s^{1/4} \lambda^{3/4}$$

Thus with increasing energy, the reduction in wavelength for the ARM at 1MeV allows interpretable resolutions to be attained to about 1.5Å with sufficient space in the objective lens to facilitate large tilting, i.e., for $C_s \simeq 3$mm. Another resolution limit is set by the ultimate cut-off of spectra resulting from instrumental instabilities. This "information retrieval limit"

is characterized by fine detail in the image beyond the Scherzer limit where the phases of the electron waves scattered by the specimen are not uniformly controlled. For this reason the image is no longer "directly" interpretable; it must be viewed with accurate knowledge of the complete contrast transfer characteristics of the objective lens and specimen conditions (thickness, orientation, etc.).

The (ARM) has been designed to meet the above requirements over its entire 400kV to 1000kV accelerating potential range, i.e., at roughly constant $C_s\lambda$ values. Consequently, the microscope can be tuned to a voltage that is below the threshold for knock-on damage in most specimens of interest and can be used to directly image its contiguous atom structure. On the other hand, ionisation damage is reduced by working at the highest voltages and this is important in many beam sensitive materials.

The key to the variable-voltage atomic resolution performance of the ARM is its top entry objective stage, which, in addition to 40° biaxial tilting, essential for high resolution studies of interfaces, incorporates a height (z) control to alter specimen position along the optic axis over a 2mm range within the objective lens. Using the z control to focus the specimen, the microscope can be operated at the appropriate objective lens current which maintains a constant $C_s\lambda$ product for any accelerating voltage. This principle is in fact put into operation automatically on the ARM; the instantaneous orientation of the specimen is furthermore displayed via a graphics software package on the monitor screen.

Moreover, the z-control stage enables the specimen to be lowered within the lens pole piece to such an extent that the pre-field of the objective can be used as a probe-former. In this way, convergent beam electron diffraction (CBED) patterns can also be recorded from the same specimen areas imaged at high resolution, providing greater precision in diffraction studies through

the analysis of higher order Laue zone (HOLZ) lines, and also permits specimen thicknesses to be measured. These data are essential in image interpretation.

Another effect of the height-adjustable stage is its influence upon the optical properties of the objective lens. In general, the lens spherical aberration coefficient decreases with increasing lens excitation although the exact functional variation is not a simple one. At higher excitation, the lens focal length shortens, making it necessary to drop the specimen deeper into the focusing field. The most serious complication of this process is that the lens is physically constricted nearer the pole piece gap, and this in turn reduces the maximum tilting range of the specimen goniometer. In the ARM, the specimen in its lowest z position is "restricted" to an otherwise generous 25° tilting range.

In addition to the microscopes, the computing and image simulation facilities at the Center provide very rapid feedback to the researcher. Such facilities are essential in order to interpret atomic resolution images, and to use the ARM effectively. Section 5 describes these facilities at the Center.

4. Some Examples of Current Research

Experimental Imaging

Since the understanding of atomic configurations at interfaces is critically important in practically all problems of materials science, direct studies of interfaces are being vigorously explored on high resolution cross-section specimens using the ARM and in combination with image simulation to assist in interpretation.

A. Metal-Compounds Semiconductor Contacts

The Al/GaAs system is of special interest because of its potential use in high speed logic, integrated optics and microwave applications as Schottky contacts. A detailed knowledge of the geometric and electronic structure of the interface is a fundamental prerequisite for understanding the electrical

properties of the contact. It is evident from several studies that the electrical charactertistic of a Schottky contact is determined within an interface region only a few atomic layers thick. A method for fabrication of a contamination-free interface is absolutely necessary and molecular beam epitaxy (MBE) offers such a possibility.

Al and GaAs are both cubic materials with face-centered and zinc-blende structures, respectively. Since the Al lattice constant is smaller than that of GaAs by almost exactly a factor of $\sqrt{2}$, there is a very good lattice match between the ideal (100) planes if the Al is rotated azimuthally 45° relative to the GaAs. Such an epitaxial relationship would be expected. However, reflection high-energy electron diffraction (RHEED) has revealed three different Al orientations on (100) GaAs, viz., Al(100), Al(110), and Al(110)R (rotated 45° to the previous one). The reason for the nucleation of grains with these different orientations is still not clear. Therefore, an investigation of the dependence of the deposition parameters, substrate temperature and the GaAs surface reconstruction on the Al growth and thus the influence on the electrical properties of Al/GaAs Schottky contacts, is being pursued.

In the particular example shown in Fig. 1 (courtesy of Dr. Liliental-Weber), Al was deposited by MBE (base pressure $<1\times10^{-8}$Pa) on a (2x6) reconstructed (100) GaAs surface at a rate of 0.5Å/sec. A substrate temperature of 25°C was maintained during deposition. The observed orientation relationship is {100}Al||{100}GaAs. For the cross-section shown on the picture {100}Al||{110}GaAs with {010}Al||{1$\bar{1}$0}GaAs and {001}Al||{001}GaAs is observed. The image suggests that diffusion of the substrate atoms into Al occurs within 8-10Å. Such an interfacial region is suggested as the area of Schottky barrier formation. Surface steps (one on the right-hand side) can play a significant role in the properties of Al contact on GaAs.

B. Precipitation Symmetry in Al-Ge

In a separate project, Dahmen and Westmacott (e.g. Ref. 9) are carrying out a detailed investigation of precipitation including the analysis of symmetry and orientation relationships on morphology (10,11). Such studies can lead to a better understanding of problems related to epitaxy and stability of compound (layered) films such as the interface problem illustrated above for Al/GaAs.

An example is furnished from analysis of the precipitation of Ge(DC) from Al(FCC). For example Al-3wt% Ge can be heat-treated by quenching from 450°C. followed by aging at 250°C to yield directly germanium precipitates in the matrix usually, but not exclusively, in the form of needles. Since the atomic volume of germanium is about 36% larger than that of aluminum, nucleation is extremely difficult and requires excess (constitutional) vacancies (9). As a result many morphologies are observed, and also all particles are twinned so as to accommodate misfit stresses. Two examples are shown in Figs. 2,3. Although there is no unique orientation relation in each case, there is a common [001] Al||[110]Ge forming an invariant line which can favor needle-like growth(12). The actual morphology is then characterized by a particular symmetry, e.g., orthorhombic, tetragonal, monoclinic. In Fig. 2, the long facets are (111) Ge parallel to (310)Al with only one common two-fold axis. The overall symmetry is 2/m, i.e., monoclinic, but interrupted by the internal twins. The resolution of the atomic columns is excellent in both matrix and particle. It is interesting that the matrix is apparently strain free around this needle, however the needle itself is twinned.

An unusual example which has been analyzed in detail in Ref. 12 is shown in Fig. 3, and summarized in the following. Five wedge-shaped sections radiate from a common center of a precipitate that is roughly circular in cross section. The five sections meet along planar twin boundaries indicated

by lines drawn on the image. The {111} twin planes in the diamond cubic structure of germanium enclose an angle of 70°5. Five such sections are therefore insufficient to fill a complete circle. The closure failure of 7.5° is taken up by two extra lattice planes inserted radially and ending at the arrow marks. A slight relative rotation between adjacent segments results from these extra planes, and these defects are perhaps more appropriately described as wedge disclinations (13). The particle appears to have pentagonal symmetry, but closer inspection reveals that its morphological symmetry is mm2, one of the three orthorhombic point groups. This symmetry describes its entire substructure, including the two extra half planes, as well as the shape.

The pentagonal twinning observed in this Al-Ge system is different from that frequently found in small particles of gold and silver, e.g., Fig. 4 with decahedral and icosahedral morphology. The multiple twinning in these particles is due to an anisotropy in surface energy: when twinned in a decahedral or icosahedral configuration, the particle surface consists of low-energy {111} facets only. The savings in surface energy more than offsets the energy of the additional twin boundaries necessary for this morphology above a critical particle size of about 5 to 10 nm (14).

There is one substantial difference between the present and earlier examples of fivefold particle symmetry. The symmetry in the germanium particles develops during a solid-state treatment close to equilibrium. In contrast, the decahedral and icosahedral multiply twinned gold and silver particles, which have been produced by vapor deposition onto various substrates as in Fig. 4, are grown under conditions far from equilibrium. Similarly, the recently discovered quasi-crystals, which exhibit icosahedral point symmetry but no translational symmetry, first observed in aluminum-manganese alloys (15) and in other materials (e.g. 16), are formed only under conditions of extremely rapid cooling, for example, splat

quenching. Tenfold twin domains similar to the fivefold configuration observed in the present work have been found in nickel-zirconium and iron-aluminum alloys with orthorhombic and monoclinic crystal structure, respectively, but only under conditions of rapid quenching (17,18).

C. Polar Semiconductors

Unlike silicon and germanium, crystalline compound semiconductors are polar. The technologically important III-V semiconductors (e.g., GaAs and InP) adopt the zincblende structure with alternating {111} planes of cations and anions. Thus, the atom column pairs which appear in the <110> projection are asymmetric "dumbells". Shown in Fig. 5 are <110> images of chemically thinned InP taken at 1 MeV in the ARM (~Scherzer defocus, -52 nm; thickness $\lesssim$10 nm). The high magnification image is an enlargement of a region within ~3 nm of the specimen edge (19). Under these conditions computer simulations show that the darkest end of the dumbell corresponds to the In column. A corresponding asymmetry is also observed in the + and -g (111) reflections in the diffraction pattern, as shown in Fig. 6. This asymmetry in diffracted intensities (i.e., lack of inversion symmetry) is only found in very thin crystals in orientations which are non centrosymmetric. Image simulation work (see Section 5) shows that interpretation of these images is only possible for a relatively narrow range of specimen thicknesses and objective lens defocus conditions and emphasizes the need for extreme care in this type of atomic imaging.

5. Computer System for Analysis of Electron Micrographs by Processing and Simulation (20)

The goal of image analysis in electron microscopy is to extract from the image (or series of images) all desired information about the specimen. In order to obtain this information, two complementary techniques are employed: image processing and image simulation. Image processing has a number of uses in electron microscopy; as well as its use in reducing noise in electron

micrographs by spatial averaging (21), it can be used to detect and display certain spatial frequencies by producing processed versions of the original image that emphasize the effects of these frequencies; most importantly, it can be used to combine the different spacings that are present in a through-focus series of micrographs (since the upper and lower limits of the spatial frequency pass-band of the objective lens change with change in focus) in order to obtain a higher overall resolution than that present in any single micrograph in the series (22,23). In a complementary way, image simulation can be used to produce a computed representation of the image that will be obtained in the electron microscope from a given specimen under specified imaging conditions (24). Such a simulated image can be compared with an experimental micrograph in order to determine the validity of the model used to represent the specimen structure. Because processed micrographs can lead to suitable model structures to be used in image simulations, and in turn, image simulations can indicate optimum processing directions, the preferred procedure is to make use of both techniques.

For the image analysis facility at the NCEM, a system is required that is both capable of easy use by external users of the facility, and yet sophisticated enough to provide the users with all necessary processing and simulation facilities whilst undergoing continual upgrades designed to incorporate improved imaging algorithms and programming techniques. Available image simulation packages such as SHRLI (24,25) do not take advantage of any special hardware available, since they are written for general computer systems and require only a minimum of standard software and hardware (a Fortran compiler, and a lineprinter capable of overprinting). In order to take advantage of available hardware at the NCEM, a new system-dependent image simulation package was written, based on experience both with programs written at Berkeley (26) and with SHRLI. For image processing software we chose SEMPER (27), as this suite of programs can be modified to take advantage of any special hardware available.

The system hardware falls into several groups (Fig. 7), and is similar to that used in the image processing system described by Saxton and Koch (28). The host is a microVAX II computer with 7MB of memory, a 71MB Winchester disk (RD53) for storage of program and operating system files, and provision for disk backup onto tape (TK50) and floppy disk (RX50). Data storage (mostly images) is provided by a 503MB Winchester disk (QDA50/61), with backup onto 9-track tape via a 6250/1600bpi tape drive (Kennedy 9400). Display of both simulated and processed images is with a two-user Gould IP9527 with the ability to display an area of 1024 x 1024 pixels (picture elements) at each of two work-stations and a total of 16MB of memory leading to a maximum image size of 4096 x 4096. In addition to its display function, the IP9527 has the ability to process images and to display their intensity histograms. For processing of images, SEMPER is used to adjust image magnifications and contrasts to facilitate on-screen comparisons of processed and simulated images. For image simulation, the new program package (named CEMPAS for Center for Electron Microscopy Processing and Simulation) provides an interactive milieu via a mouse input. At a graphics terminal, the user can open a CEMPAS menu to create atom position files, to view the crystal unit cell from any specified direction, to simulate the dynamical diffraction process for any specimen thickness or tilt, and to display the resultant simulated electron wavefield under any selected microscope conditions. In addition, it is possible to display simulated electron diffraction patterns and diffractograms, plots of CTFs (linear-image Contrast Transfer Functions), and plots of variation in diffracted beam intensities with specimen thickness. In order to keep processing and simulation times reasonably short the simulation computation relies heavily on the attached array processor (CSPI MM+4).

With the hardware outlined above, images are quickly simulated using arrays of sizes up to 1024 x 512 in the diffraction calculation (arrays of 1024 x 1024 or larger require the input of data to the CSPI during the calculation, and take somewhat longer to compute). Diffraction (multislice) calculations using the CSPI require only a few minutes time, compared with the several hours that would be required using the microVAX alone.

In association with the image processing computer, a second system has been designed to acquire and enhance electron microscope images in real time at video rates from three electron microscopes. This real-time system uses a second microVAX II host computer linked to the main host via ethernet connectors (DEQNAs and DELNI). The image grabber/enhancer for each electron microscope consists of three VME cards (DataCube Max-Video) in a VME-bus back-plane connected to the Q-bus through a bus converter. Each grabber/enhancer has the ability to digitize images at video rates, to time-average the image signal in order to reduce noise, to store and display the image, and to change its contrast. In addition to the grabber/enhancers, a small array processor (Mercury ZIP3232 with 2MB memory) is present on the VME-bus to provide the electron microscope operator with diffractograms of real-time images with a lag-time of approximately 1.5 seconds. One advantage of placing the image grabbers on the same VME bus as the array processor, is the much higher bandwidth of the VME bus (rated speed of 27MB/sec) compared with that of the Q-bus (3.3MB/sec).

The simulation process commences with the formation of a model of the structure. Figure 8 shows a display of a proposed model of a metastable zirconia phase in [010] orientation (29). Here the atoms are drawn as shaded spheres (28), with the Zr atoms represented by the small spheres and the oxygen atoms by the large spheres. For comparison, Fig. 9 shows the projected potential of the structure in [010]; now the Zr atoms have the larger

projected potential and form a square lattice; the smaller peaks from the oxygen atoms in alternating rows show how they are skewed alternatively left and right (circled). From this projected potential any structure image is expected to show a square lattice of spots, with smaller spots between. Figure 10 shows what actually happens to the ideal structure image (or weak-phase-object image) as the microscope resolution is improved from 2.50Å to 2.01Å; at 2.5Å resolution (10a), a square lattice of black spots is indeed observed at the Zr atom positions, but as resolution is improved to 2.25Å (10b) and 2.01Å (10c), the columns of black spots begin to show a zig-zag mien. This effect also occurs in images simulated for the NCEM Atomic Resolution Microscope at -200Å defocus for crystal thicknesses near 300Å, where white spots occur in zig-zag columns (Fig. 11). Figure 12 is an actual image with the simulation inset. This result enabled the identification of the orientation of the oxygen atom pair to be established (29). Note that, although the oxygen atoms are not seen directly, their influence on the image is quite apparent.

ACKNOWLEDGEMENTS

The National Center for Electron Microscopy is funded by the Director, Office of Energy Research, Office of Basic Energy Sciences, Materials Science Division, U.S. Department of Energy under Contract No. DE-AC03-76SF00098. I am grateful to my colleagues for providing input to this paper, Drs. Westmacott, Dahmen, O'Keefe, Sands and Liliental-Weber for the illustrations, and to the technical and support staff for their excellent work at the Center.

REFERENCES

1. G. Dupouy, Adv. Opt. Elec. Microsc., 2, 167 (1968).
2. G. Thomas and J.C. Lacaze, J. Microsc. 97, 301 (1973).
3. D.G. Howitt, R.M. Glaeser and G. Thomas, J. Ultrastr. Res. 55, 457 (1976).
4. Proc. 7th Int. Conf. on HVEM, Eds. R.M. Fisher, R. Gronsky and K.H. Westmacott, University of California LBL 16031, U.S. Department of Commerce, Springfield, Virginia, (1983).
5. In-Situ Experiments with H.V. Electron Microscopes, Ed., H. Fujita, Osaka University Res. Center for UHVEM, November, 1985.
6. 11th Int. Congress on Elec. Microscopy, Kyoto, Japan, Vol. 2, Japan. Soc. E.M. Tokyo, (1986), p....
7. K.M. Krishnan, P. Rez, G. Thomas, Y. Yokota and H. Hashimoto, Phil. Mag. B53, (4), 339 (1986).
8. B. Jouffrey, J. Sevely, G. Zanchi and Y. Kihn, 11th Int. Congress on Elec. Microscopy, Kyoto, Japan, Vol. 2, Jap. Soc. E.M. Tokyo, 1986, p. 891.
9. U. Dahmen, A.R. Pelton, M.J. Witcomb, K.H. Westmacott, MRS Symp. Proc. Vol. 62, p. 217 (1986).
10. J.W. Cahn and G. Kalonji, Proc. Int. Conf. Solid-Solid Phase Transform. (Pittsburgh) (1981), p. 3.
11. R. Portier and D. Gratias, J. Phys. (Paris) Colloq. CA 43, 4 (1982).
12. U. Dahmen and K.H. Westmacott, Science 223, 875 (1986).
13. A.E. Romanov and V.I. Vladimirov, Phys. Status Solidi A78, 11 (1983).
14. L.D. Marks, Philos. Mag. A49, 81 (1984).
15. D. Shechtman, I. Blech, D. Gratias, J.W. Cahn, Phys. Rev. Lett. 53, 1951 (1984).

16. Z. Zhang, H.Q. Ye, K.H. Luo, Philos. Mag. A52, L49 (1985).

17. W.J. Jiang, Z.K. Hei, Y.X. Guo, K.H. Kuo, ibid., p. 153.

18. E. Louis, R. Mora, J. Pastor, Met. Sci. 14, 591 (1980).

19. T. Sands, J. Metals, Vol. 38, 31 (1986).

20. The computing and image processing facilities have been developed by M.A. O'Keefe and R. Kilaas.

21. W.O. Saxton, J. Microsc. Spectrosc. Electron. 5 661 (1980).

22. P. Schiske, in Image Processing and Computer-Aided Design in Electron Optics, P.W. Hawkes (ed.), Academic Press, London (1973) p. 82.

23. E.J. Kirkland, in Proc. 42nd EMSA, G.W. Bailey (ed.), San Francisco Press, San Francisco (1984) p. 432.

24. M.A. O'Keefe, P.R. Buseck and S. Iijima, Nature 274, 322 (1978).

25. M.A. O'Keefe, in Electron Optical Systems, J.J. Hren et al. (ed.) SEM Inc., AMF O'Hare, p. 209 (1984).

26. R. Kilaas, Ph.D. Thesis, University of California, Berkeley (1985).

27. W.O. Saxton, in Inst. Phys. Conf. Ser. No. 44, Institute of Physics, London (1979) p. 78.

28. W.O. Saxton and T. Koch, J. Microscopy 127, 69 (1982).

29. T. Bielicki, U. Dahmen, K.H. Westmacott and G. Thomas, Zirconia 1986 (Tokyo, Japan); Proc. Int. Conf. ed. T. Somiya, in press.

FIGURE CAPTIONS

Fig. 1 ARM image of cross section of Al on GaAs 1MeV. (Courtesy of Z. Liliental-Weber)

Fig. 2 ARM image of Ge needle precipitated from Al-3%Ge alloy 800kV. Note internal twinning and flat faces with {111} Ge parallel {310}Al. (Ref. 9)

Fig. 3 As Fig. 3, pentagonal twinned particle [110]Ge parallel to [100]Al. (Ref. 12)

Fig. 4 Gold particle deposited on a carbon substrate; compare to Fig. 3.

Fig. 5 ARM image of InP (1MeV). Note dumbbells at 1.5Å resolution. (Courtesy of T. Sands)

Fig. 6 [110] diffraction pattern from InP thin foil; note asymmetry in + and -g <111> reflections. (Courtesy of T. Sands)

Fig. 7 Schematic of computer system at NCEM.

Fig. 8 Proposed model for metastable orthorhombic phase of ZrO_2. (Ref. 29)

Fig. 9 Projected potential in [010] from model in Fig. 8.

Fig. 10 Weak phase object at resolutions of 2.5Å (a); 2.25Å (b); and 2.01Å (c).

Fig. 11 Simulated image of structure corresponding to Fig. 8 for thickness of 300A and defocus of -200Å.

Fig. 12 Actual ARM image of metastable ZrO_2; inset shows simulation; agreement is excellent. (Ref. 29)

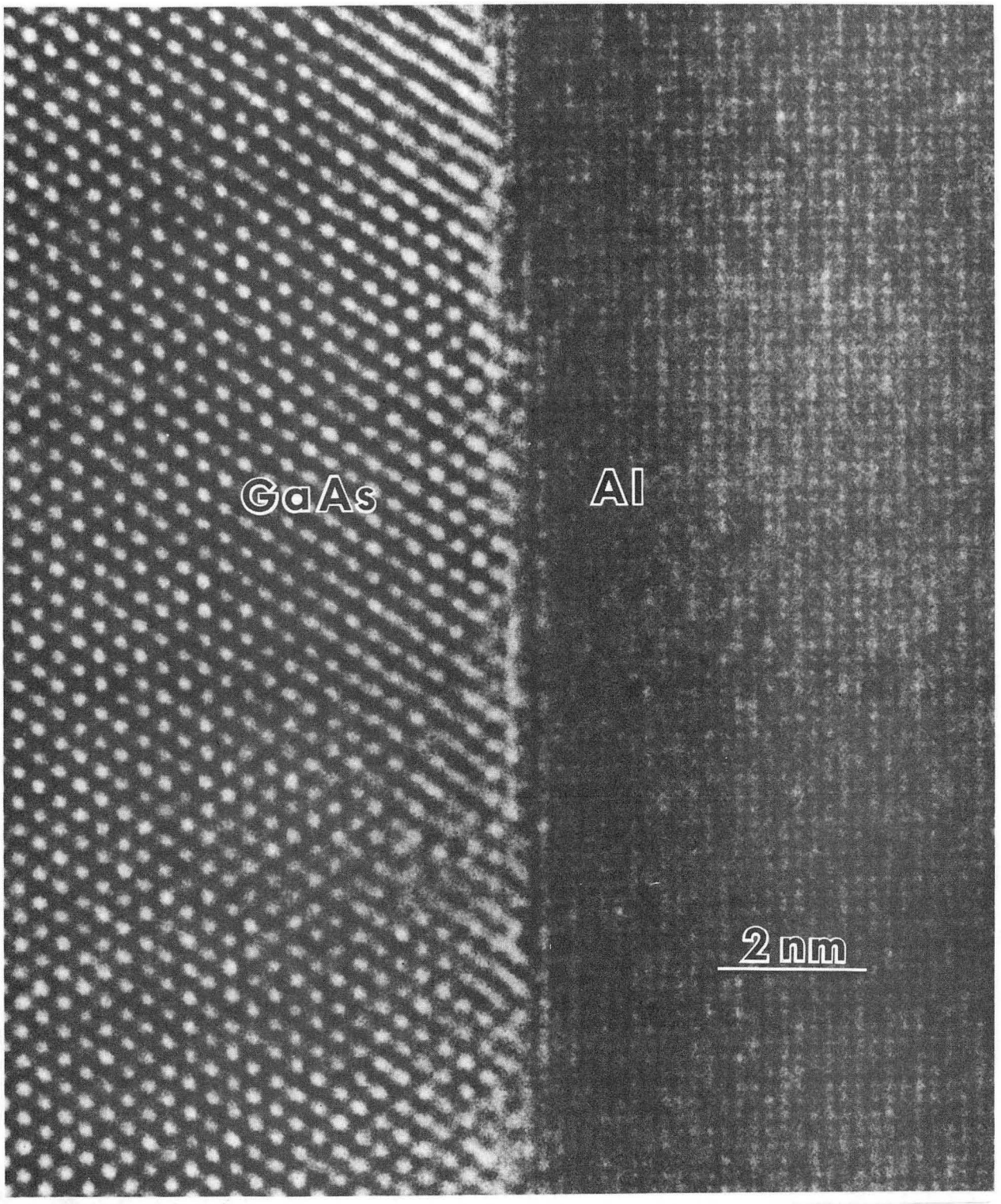

XBB 8612-9891

Fig. 1

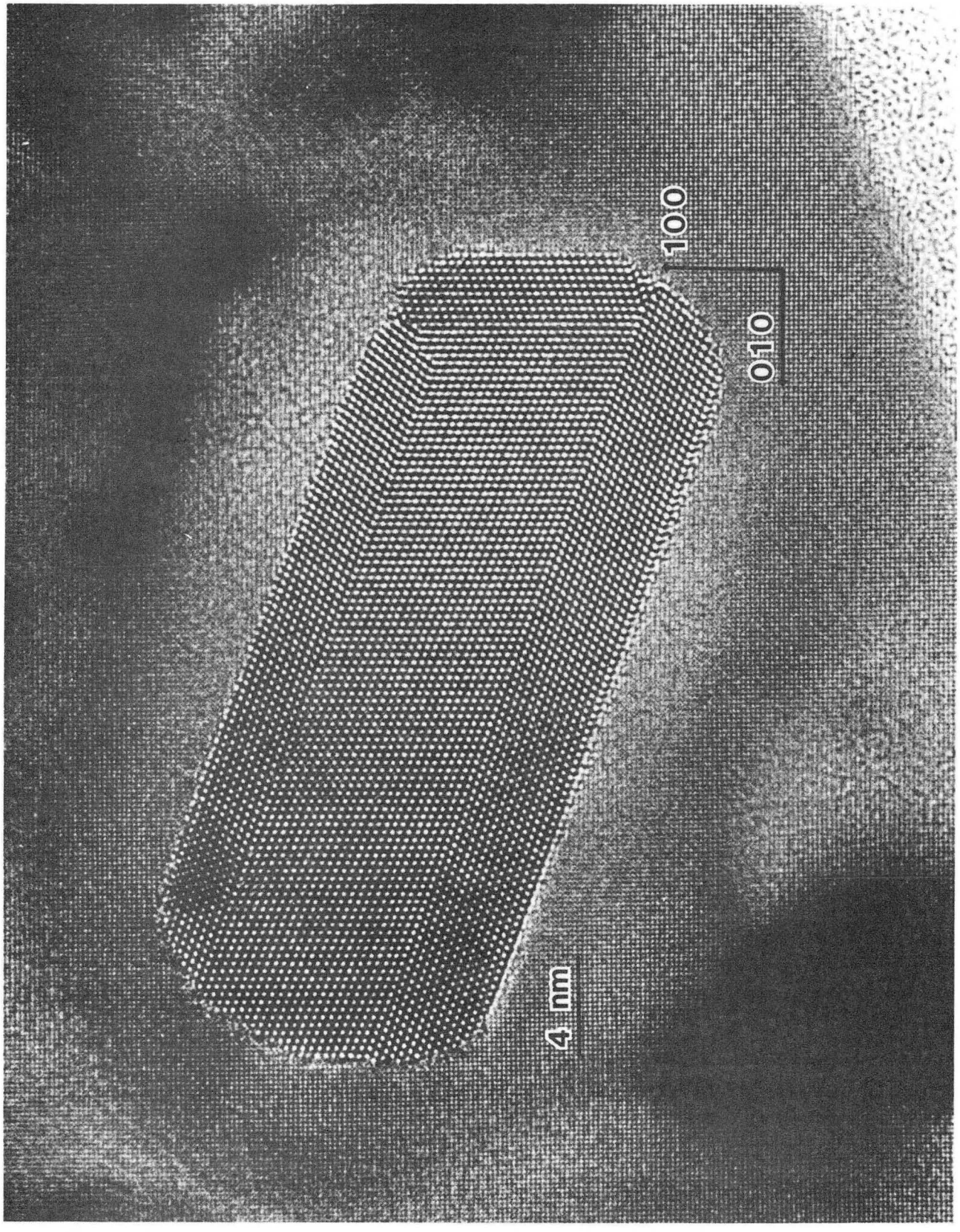

XBB 8610-8555

Fig. 2

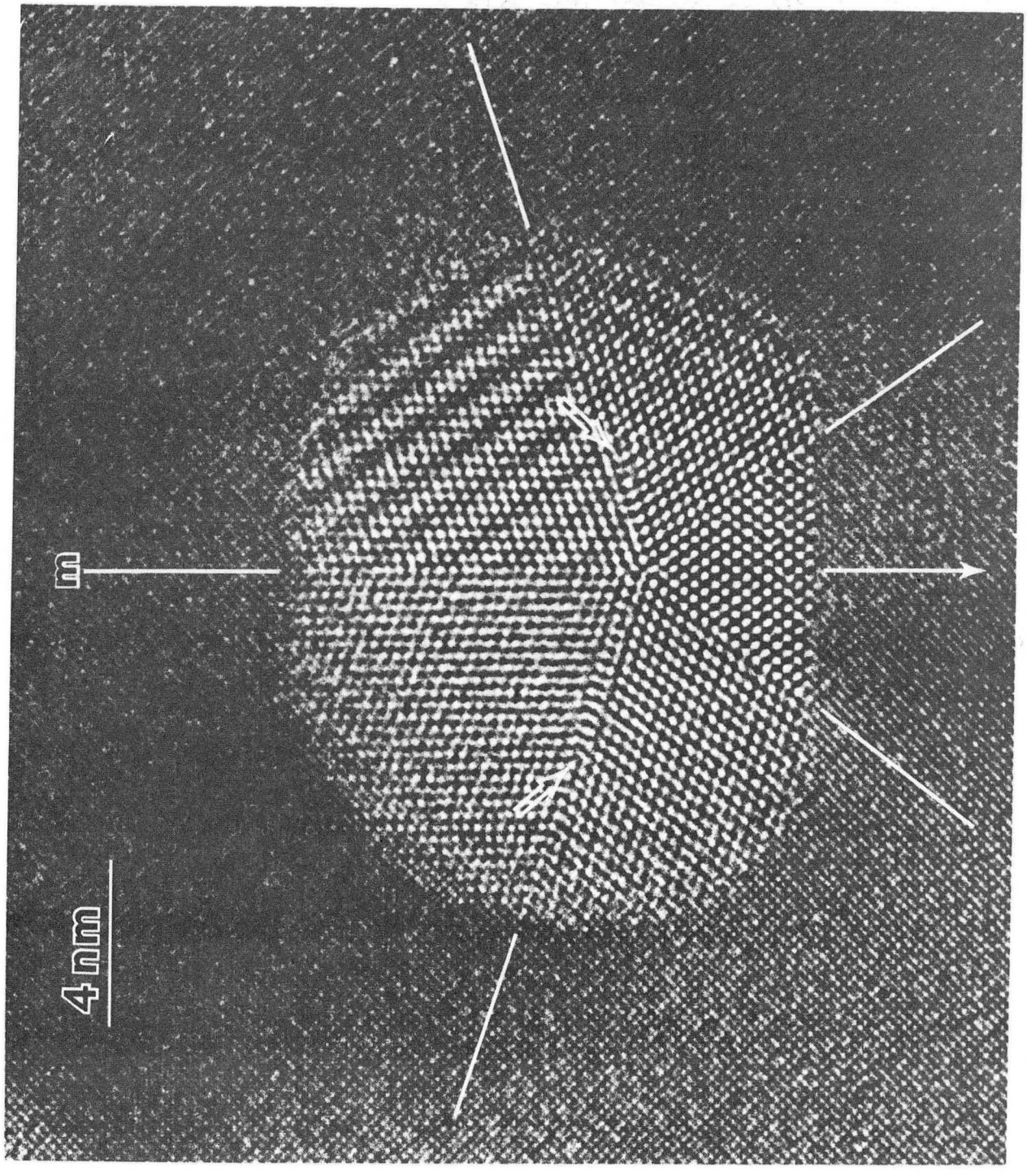

XBB 864-2117 A

Fig. 3

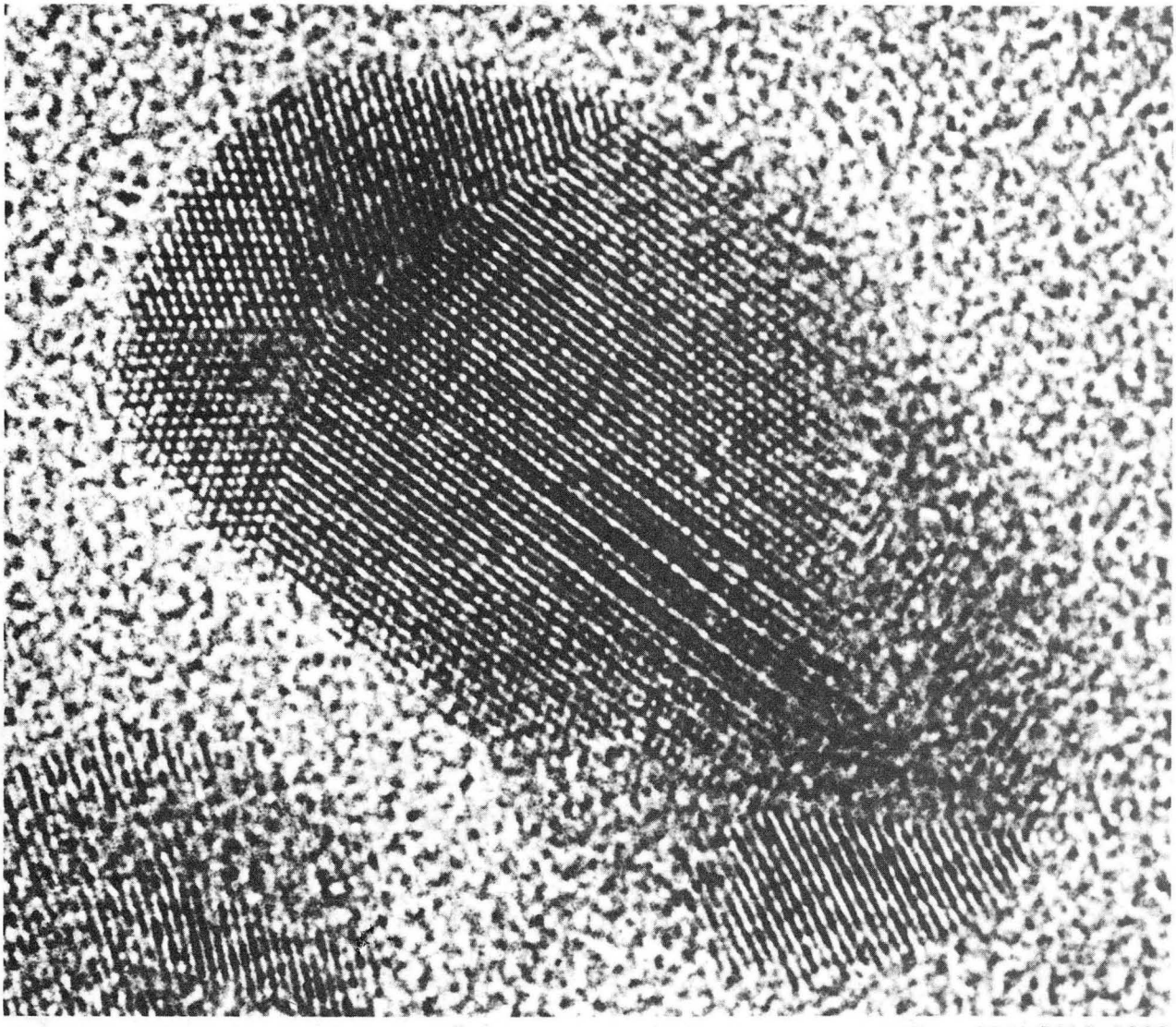

XBB 8612-9890

Fig. 4

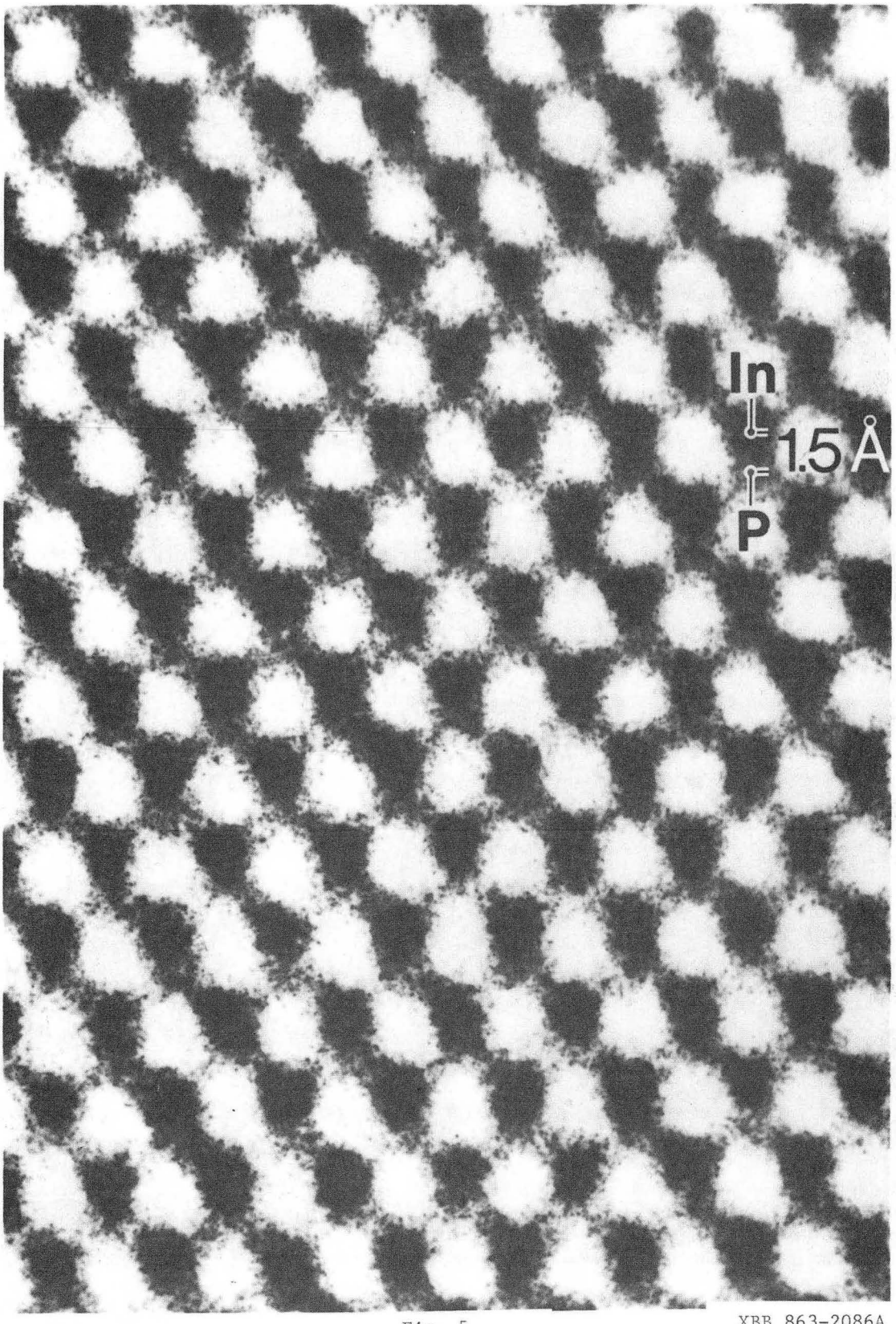

Fig. 5

XBB 863-2086A

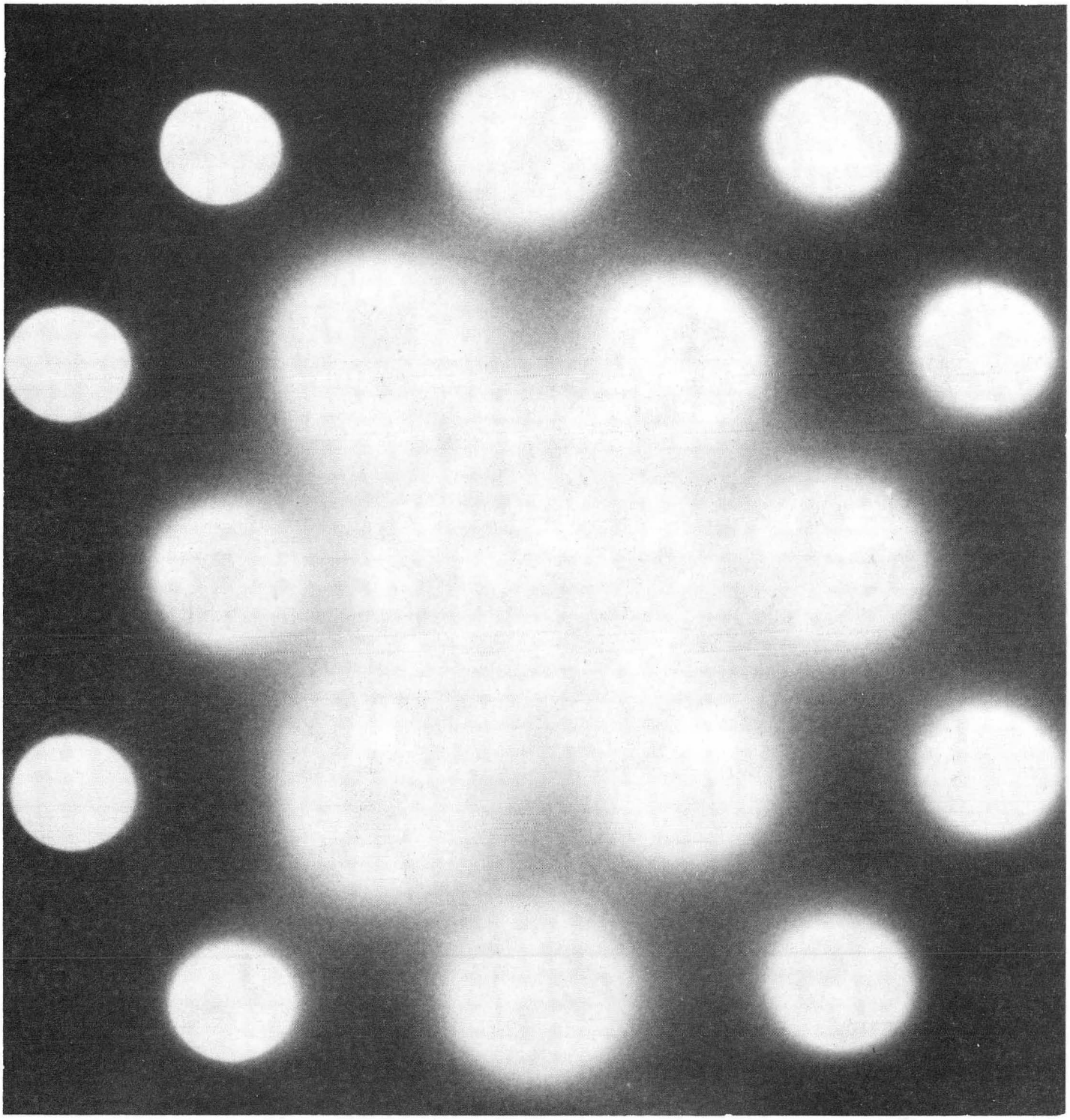

XBB 863-2083

Fig. 6

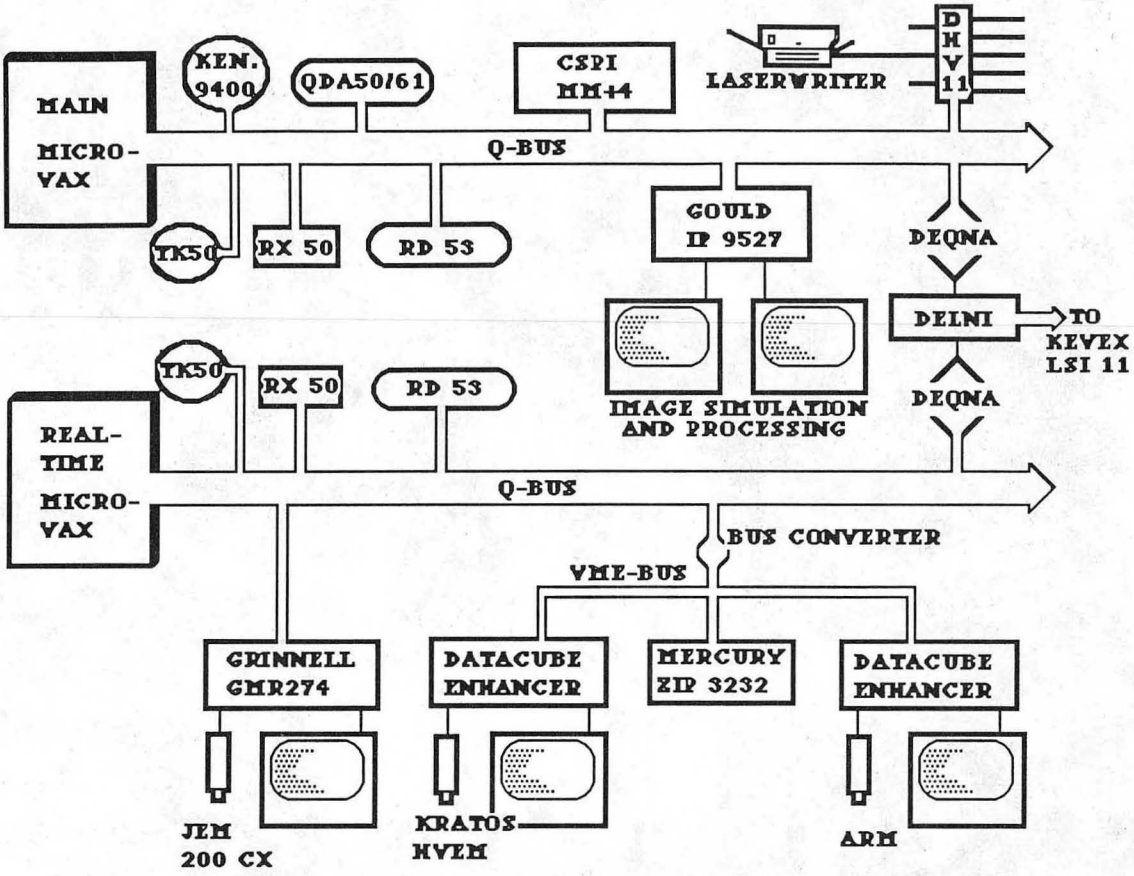
MAIN
MICRO-
VAX
KEN.
9400
QDA50/61
CSPI
MM+4
LASERWRITER
DHV
11
Q-BUS
TK50
RX 50
RD 53
GOULD
IP 9527
DEQNA
DELNI
TO
KEVEX
LSI 11
IMAGE SIMULATION
AND PROCESSING
TK50
RX 50
RD 53
REAL-
TIME
MICRO-
VAX
DEQNA
Q-BUS
BUS CONVERTER
VME-BUS
GRINNELL
GMR274
DATACUBE
ENHANCER
MERCURY
ZIP 3232
DATACUBE
ENHANCER
JEM
200 CX
KRATOS
MVEM
ARM
XBL 8611-4756

Fig. 7

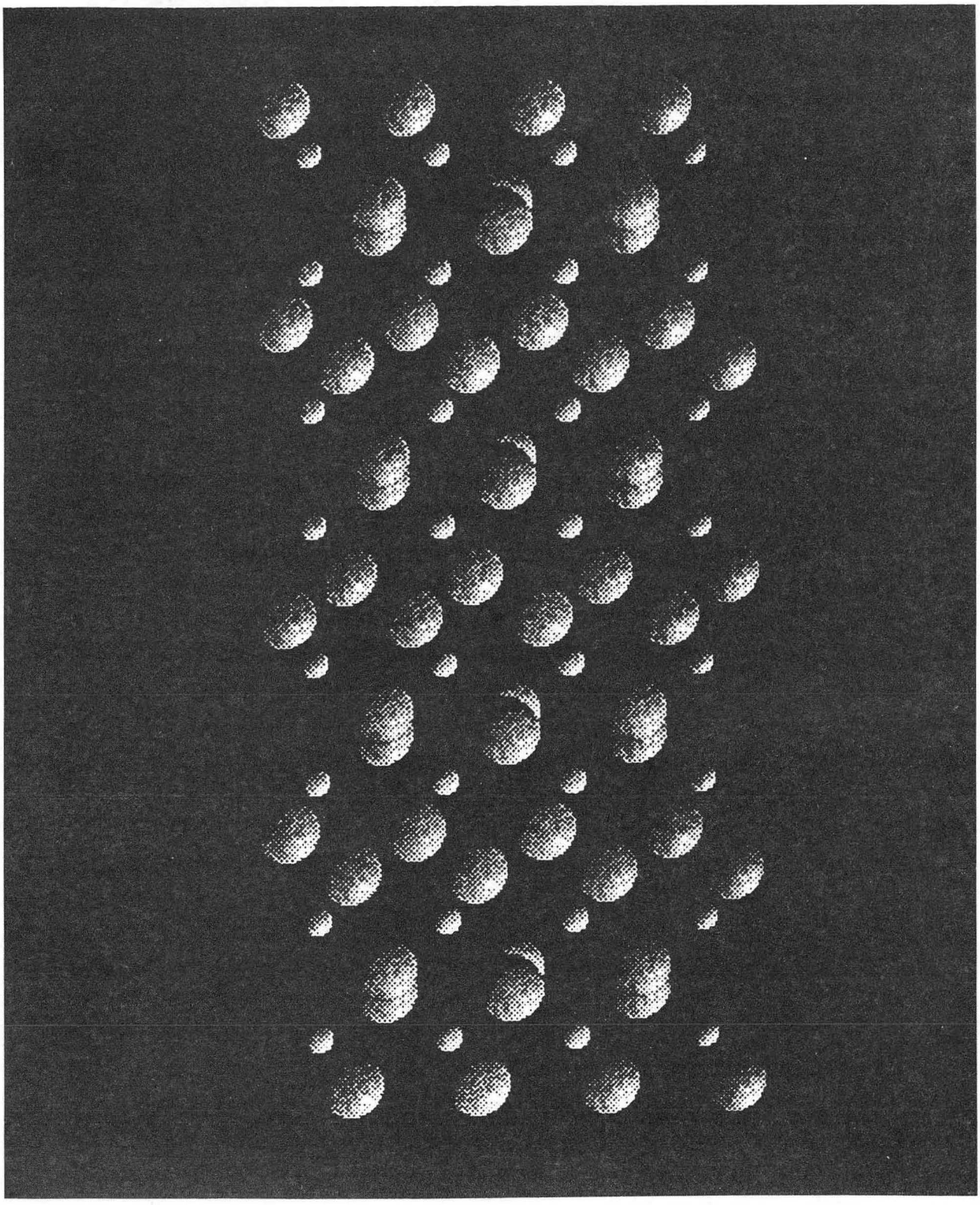

XBL 8611-4755

Fig. 8

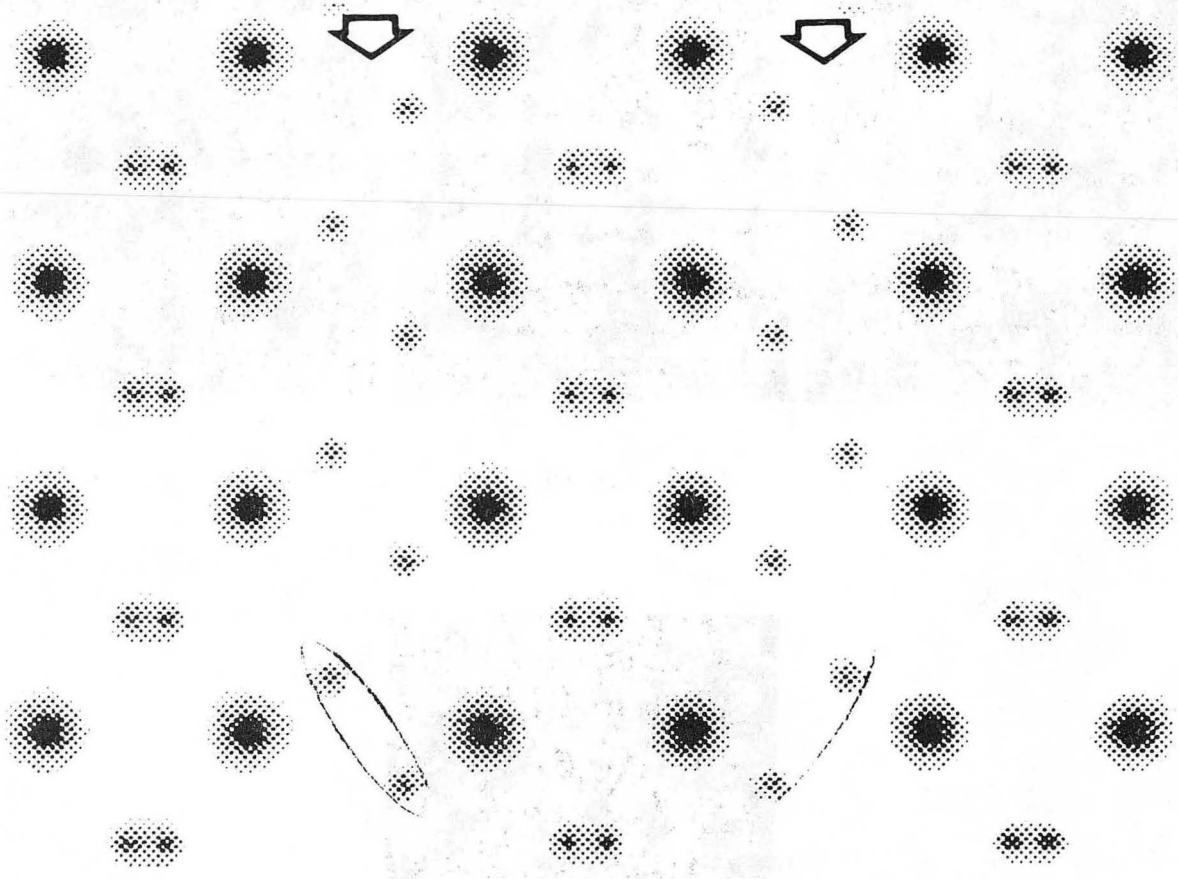

XBL 8611-4754

Fig. 9

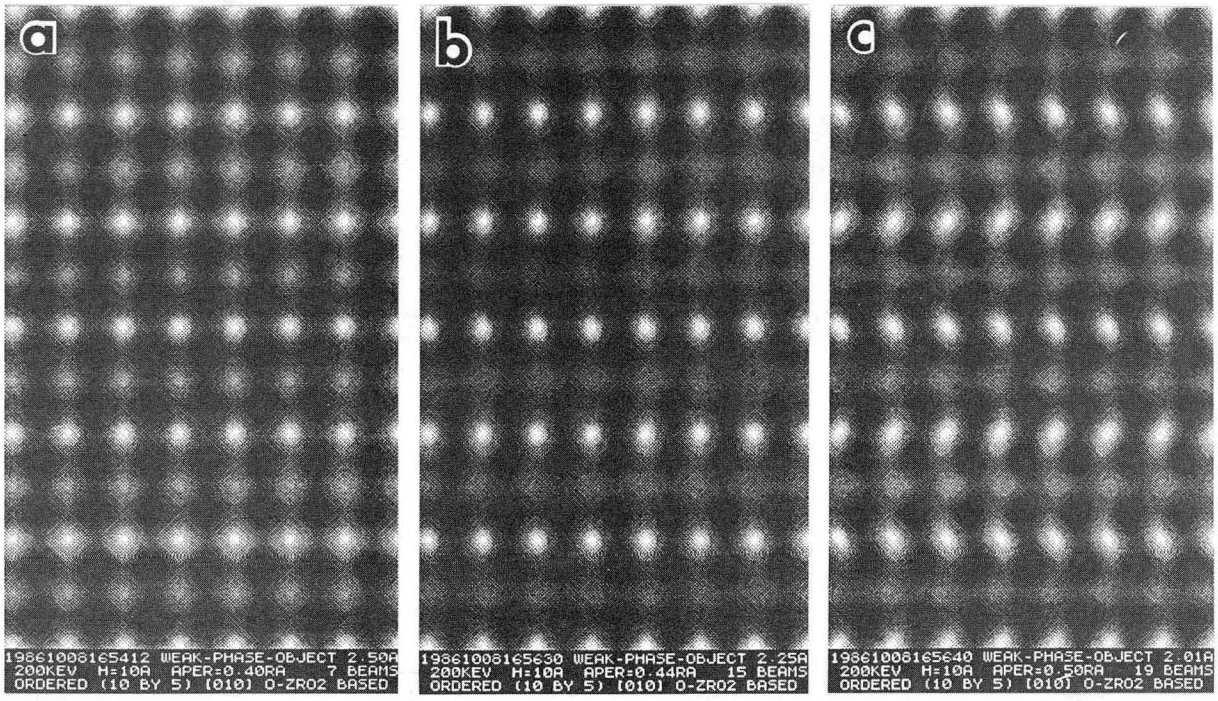

Fig. 10

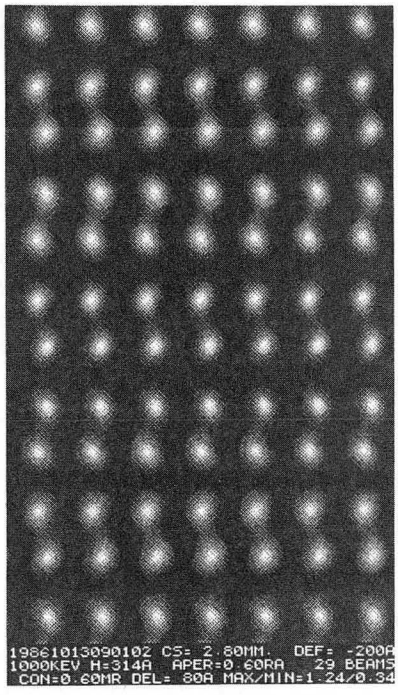

Fig. 11

XBB 8612-9889

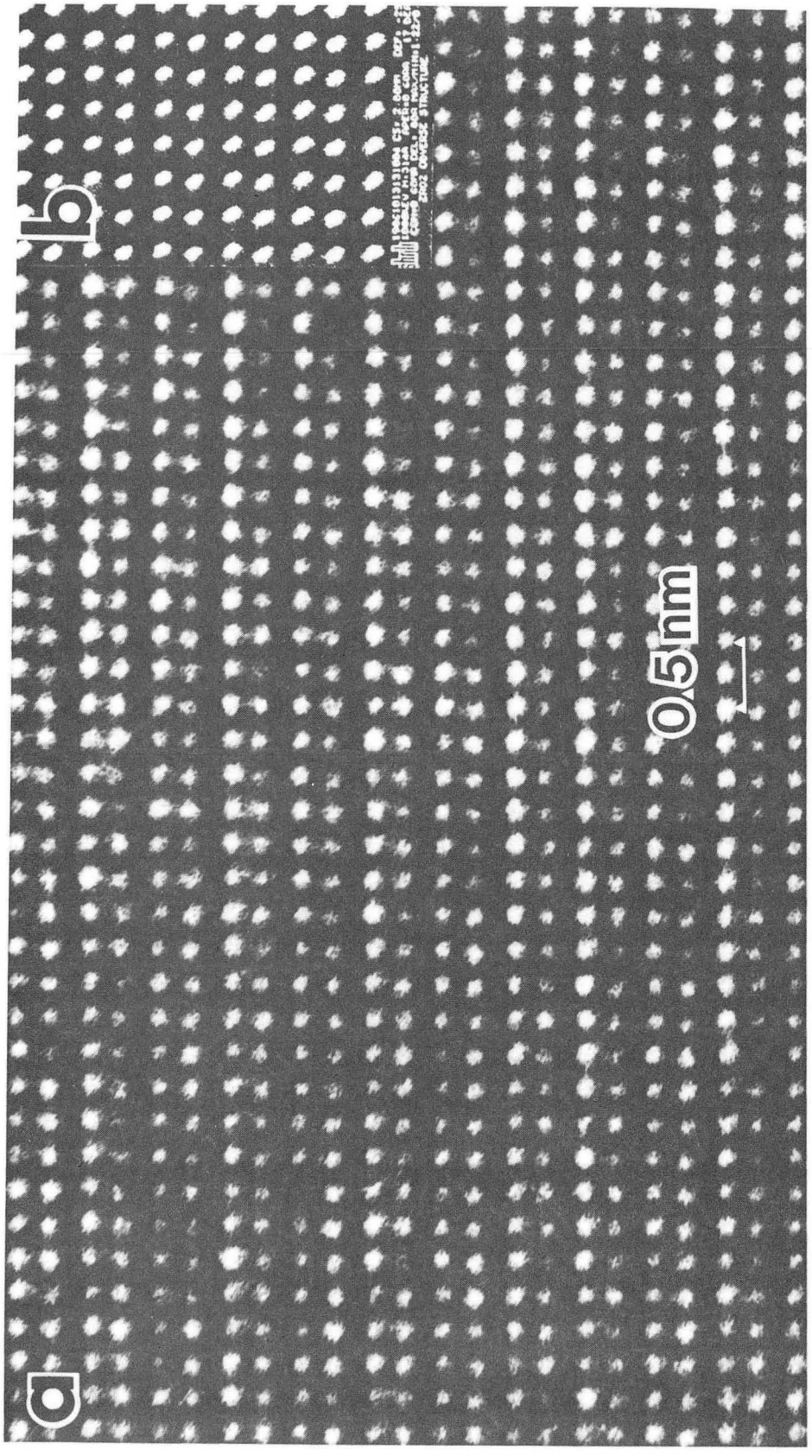

XBB 8610-8580 A

Fig. 12

This report was done with support from the Department of Energy. Any conclusions or opinions expressed in this report represent solely those of the author(s) and not necessarily those of The Regents of the University of California, the Lawrence Berkeley Laboratory or the Department of Energy.

Reference to a company or product name does not imply approval or recommendation of the product by the University of California or the U.S. Department of Energy to the exclusion of others that may be suitable.

LAWRENCE BERKELEY LABORATORY
TECHNICAL INFORMATION DEPARTMENT
UNIVERSITY OF CALIFORNIA
BERKELEY, CALIFORNIA 94720